INTERNATIONAL JOURNAL OF ADVANCE RESEARCH, IDEAS AND INNOVATIONS IN TECHNOLOGY

ISSN: 2454-132X

Impact factor: 4.295

(Volume 4, Issue 2)

Available online at: www.ijariit.com

Grain size and corrosion investigations on friction welding of AA6061-T6 Al alloy to Cu with Ni interlayer

E. Ravikumar
ramakrishnar2009@gmail.com
Alpha College of Engineering, Chennai, Tamil Nadu

N. Arunkumar
n.arunkumar@erdiffmail.com
St. Joseph's College of Engineering, Chennai, Tamil Nadu

D. Anandabadmanaban
ananth_1out@yahoo.com
Sri Sivasubramaniya Nadar College of Engineering, Chennai, Tamil Nadu

ABSTRACT

In this study, Cu – Ni- Al 6061, rod were joined by friction welding techniques at various mechanical characterisation. Corrosion, micro, macrostructure, grain structure, scanning Electros ion Micros cope[SEM] Analysis behavior of the Explosively joined sample was investigated. The influence of grain size on pitting corrosion of 6061Al in 3.5wt NaCl solution was investigated by electrochemical methods. At the end of the corrosion test carried out according to ASTM G3- Standard no separation was observed at the interface of the joint samples. The result of corrosion test showed no sign of any distinctive separation crack, tear, in the interface. The highest corrosion rate was measured in regions next to interfaces, the optical microscope and SEM examinations revealed that the corrosion current and corrosion rates are very low for the specimens welded with low upset pressure compared to other specimens. The minimum and maximum corrosion rates vary from0.466 and 356.64 mA/ Square centimeter.

Keywords: *Friction welding, Corrosion rate, Optical microscopy, Corrosion rate, SEM, Pitting corrosion.*

1. INTRODUCTION

Nickel-aluminum copper is generally two-phase, duplex alloys containing 5% to 11% aluminum as well as additions of iron and nickel for strength. Increasing the aluminum content results in higher strength, which is attributable to a hard, body-centered-cubic phase, which enhances properties of castings as well as hot working in wrought alloys. The other alloying elements also improve properties and alter microstructure. Specifically, nickel improves corrosion resistance, while iron acts as a grain refiner and increases tensile strength. Nickel also raises yield strength and both nickel and manganese act as microstructure stabilizers. Nickel-aluminum bronzes are metallurgically complex alloys in which small variations in composition can result in the development of markedly different microstructures, which can, in turn, result in wide variations in seawater corrosion resistance. Those microstructures, which result in optimum corrosion resistance, are obtained by control of composition and heat treatment.

Copper nickel-aluminum alloys are very corrosion resistant and thermally stable. The copper-nickel alloys contain from 2 to 30% nickel depending upon the application. These alloys usually have additions of iron, chromium, niobium, and or manganese to improve the strength and corrosion resistance. They are virtually immune to stress corrosion cracking and exhibit high oxidation resistance in steam and moist air. The copper-nickel alloys have moderate strength even at elevated temperatures. The higher nickel alloys are well known for their corrosion resistance into marine befouling. The copper-nickel alloys are used in applications such as electrical and electronic products, tubes for condensers in ships and power plants, various marine products including valves, pumps, fittings and sheathing for ship hulls. The wrought alloys are designated as UNS C70100 through C72950. The cast alloys are C96200 to C96900. Cast copper-nickel alloys are typically used aboard ships, on offshore platforms, and in coastal power plants.

Copper-nickel alloys are single phase alpha structures because nickel is completely soluble in copper. The as-cast dendrites are heavily cored, they contain a composition gradient because the alloys freeze over a wide temperature range. The as-cast structures consist of alpha dendrites that have a decreasing nickel content from the center to the edge of the dendrite. The interdendritic regions, being the last liquid to solidify, are higher in copper. Mechanical treatments break up the dendritic structure, but even

repeated mechanical and thermal treatments do not homogenize the alloying elements. Segregation of the alloying elements, which starts out as coring of the dendrites, is seen as banding in the wrought microstructures. The microstructure of the wrought materials is similar to that of unalloyed copper, it consists of twinned grains of alpha copper. The banding of the alloying elements shows up as dark rows or stripes across the grains.

6xxserious aluminum alloys are widely used in aerospace industries for their low density and favorable mechanical properties [1]. However, these alloys are often suffered from pitting corrosion and stress corrosion cracking when subjected to aggressive environment such as salt water spray and salt fog[2,3].Friction welding process can minimize the formation of the brittle intermetallic compound at the interface because it is carried high pressure, short processing time and below melting temperature [3]. Garcia et .al studied the pitting corrosion resistance of different zones of the welded joints of austenitic stainless steels[AISI304316L] in an acid solution containing chlorides by potentio dynamic anodic polarization and cyclic potentiodynamic polarization, and it is shown that pitting corrosion of weld metals was higher than that of base metal [4]. Bimes et al studied the pitting corrosion behavior of spurmartenstic weld in chloridesmaintaining potentiatstic, technique and pointed out that HAZ was the most critical zone for pitting corrosion and the base metal was in the noble zone [5]. The AA6061 alloys contain major addition zinc, along with the magnesium or magnesium plus copper and nickel that developed a various level of strength. Those containing copper and nickel have the highest strength and have been used as construction materials and food industries, air craft's for more than50 years [6]. Among heat treatable alloys, those of 6xxx, which are moderate strength alloys, provide a high resistance to general corrosion equal to approaching that non- heat treatable alloy [7]. Therefore, it is necessary to study the corrosion behavior of Al-Ni-Cu Interlayer in Alkaline condition. Aluminum when joined with Copper gives intermetallics.Intermetallic formation acts to reduce corrosion resistance.So, it is very much necessary to improve corrosion at the interface between Aluminium and CopperHence, an interlayer has to be added to Aluminium and Copper.From a careful study of the Periodic Table, Nickel is chosen as the interlayer.Nickel is close to Copper in the periodic Table and it also aids in improving corrosion.Although, the concept of the interlayer is not new, use of Nickel as an interlayer has not been tried much, especially for frition welding of non-ferrous combinations.

2. ABBREVIATIONS AND ACRONYMS

3.5% NaCl solution	g of NaCl per 100-g of solution (=0.6 M)
ASME	American Society of Mechanical Engineers
ASTM	American Society for the Testing of Materials
CE	Corrosion Electrode
Current density	Corrosion Current Density in [mA/cm2]
E_{CORR}	Corrosion potential in mV
EDX	Energy Dispersive X-ray (analysis)
FRW	Friction welding
HAZ	Heat Affected Zone
I_{CORR}	Corrosion Current in mA
mA/cm^2	Current Density in milli-Amperes per square centimetre
mm/year	Corrosion Rate in millimeters per year
MPa	Pressure in Megapascals
mV	Millivolt
pH	a measure of the hydrogen ion concentration of a solution
RE	Reference Electrode
RPM	Rotational Speed of revolutions per minute
SCEAqua Regia	Saturated Calomel Electrode used as Reference Electrode (=RE) A mixture of one part Nitric Acid and three parts Hydrochloric Acid
FESEM	Field emission scanning Electron Microscope (fractography)
WE	Work Electrode

2.1 EXPERIMENTAL WORK

Wrought aluminum alloy AA6061 and pure copper and nickel with a Dia of 19mm were used for the present study [8]. The Chemical composition and mechanical properties of base metals and Nickel interlayer are presented in Table 1, Table 2 and Table 3. The joints are fabricated by the TaguchiL9 orthogonal array at three levels and four parameters as shown in Table 4. The 4 samples which gave the reasonable value of selected for the corrosion test, microstructure, macrostructure, and SEM. For micro structure evaluation inverted metallurgical optical microscopy with range 100 - 600x was used. Annealed specimens were mechanically polished using sand papers and diamond pastes and then were etched by3.5% nital and an aqueous solution of 100g/L Sodium metabisulfite.The microstructure of the specimen was observed in the optical microscope. The corrosion properties of each specimen were evaluated through immersion and electrochemical polarization tests in a neutral aqueous through a solution of 4% wt of NaCl.Specimen for immersion test measuring 75 mm length and 19mm dia were polished using the diamond particle of 1µm, and ultrasonically cleaned in acetone, followed by weighing using a digit electronic balance with a precision of 1/10,000 before weight loss test, the corroded specimens were rinsed with distilled water. The corrosion product was removed using a smooth brush, then rinsed and dried again. The weight loss of each specimen during the 24-h immersion test was measured to calculate the corrosion rate.

In order to study corrosion, potentiodynamic polarization test was conducted as per the standard ASTM friction welded dissimilar aluminum alloys weld joints. The welded samples are interface junction was compared with parent metal. In this type of corrosion saturated calomel electrode was used as reference electrode. Photograph of the experimental set up is shown in Figure1

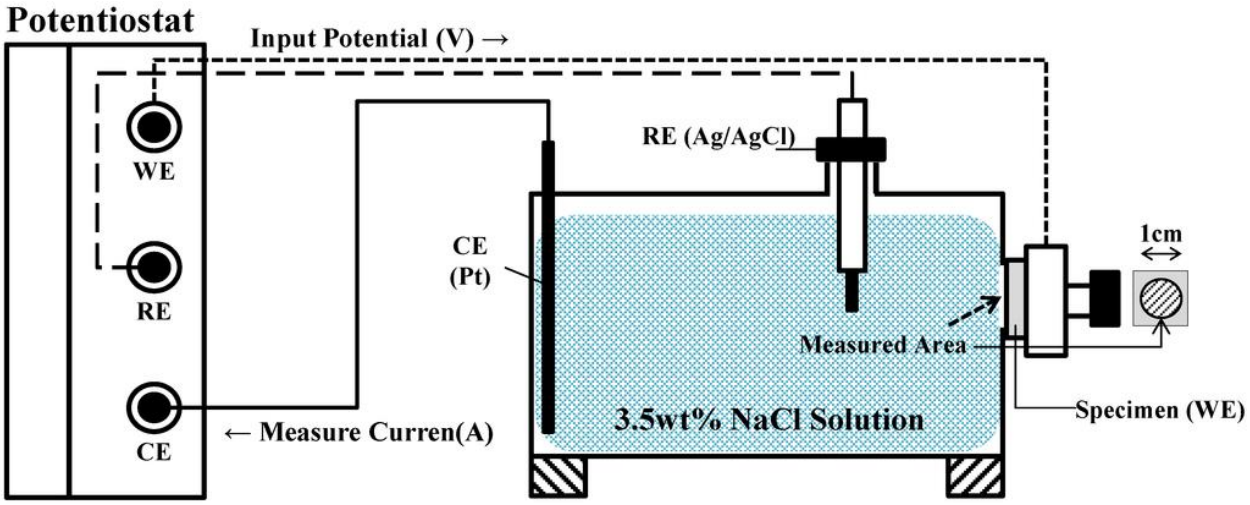

Fig.1: Experimental test set up-Label the setup

Potentiodynamic polarization tests were carried out according to the ASTM standard G3–89, using software based ACM GILL AC Potentiostat. The flat type working electrode of the AA6061-T6 aluminum alloy base metal and different weld zones, a saturated calomel electrode coupled to a fine Lugging capillary as a reference electrode, and a platinum electrode as a counter electrode, was used. The Lugging capillary was kept close to the working electrode to reduce the ohmic contribution. The polarization curves were determined by stepping up the potential at a scan rate of 0.5 mV sec^{-1} from –250 mV to +250 mV versus open circuit potential (E_{corr}vs. SCE). All the experiments were conducted at room temperature (25°C), with 60 minutes time delay to reach steady state in a freely aerated condition. During this time delay the potential Vs time, and current Vs time were also recorded. All the experiments conducted in this section were repeated at least two times for reproducibility.Friction welded samples are 1cm x1cm having a different region of base metal and the weld zone was cut from the cylindrical specimen in Wire EDM process with a thickness of 1mm. In this study, a corrosive environment 3.5% sodium chloride was used. The sample was polished by different grades of emery sheets and the impurities were removed.It is observed that corrosion resistance of weld metal is better than that of TMAZ (Thermo mechanical affected zone) and base metal to determine corrosion parameters such as corrosion potential (Ecorr.) and corrosion current (Icorr.)

2.2 Micro-Structural observations

Example microstructure of annealed for various duration times are displaced in fig. Showing a microstructure of consisting of 100% AL. The growth of recrystallized aluminum grains with annealing time is evident from the optical micrograph. The grain diameter of samples recrystallized at various timed was obtained from quantitative analysis

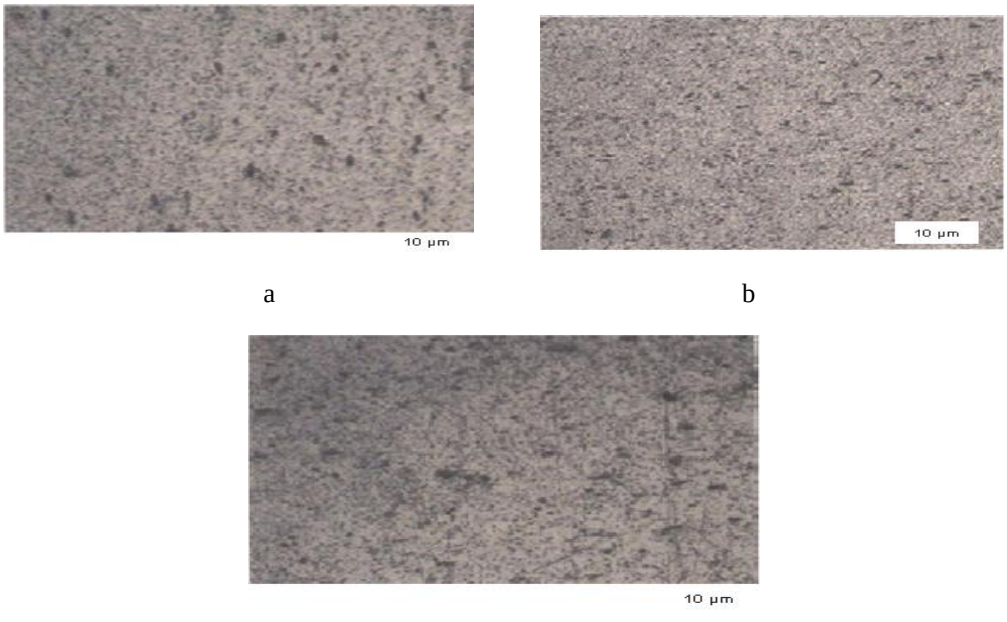

a b

c

Fig. 2. Fig Optical micrographs of AA6061 Al after recrystallization annealing at 250°c for: (a) 4min (b) 13min (c)20min

2.3 Analysis of the location of the metastable pit

The morphology of metastable pits after the electrochemical test was studied by scanning electron Microscopy technique. An SEM image of the metastable pit in sample with15.1 m grain size is shown fig.3 for instance. Clearly, pits are generated in both grain interiors and grain boundaries. The pit nucleation site was analyzed by sem microscope equipped by EDS.

The high content of the SI (0.708) Iron and silicon indicates that pits nucleate on the SI inclusion sites fig.The dissolution of the sulfide inclusion has preferably taken place close to the metal matrix[9,10] As expected, fig. shows the distribution of inclusions was not changed by recrystallization annealing time.

2.4 Pitting potential probapality

Typical potentiodynamic curves of AA6061 Al with various grain size are illustrated. The abrupt increase in current density, which is observed following the metastable pitting activity in the passive region of potentiodynamic test, is an indication of stable pitting corrosion in all specimen. As shown in fig 2,3,4, there was no distinct difference in pitting potentials and passivity current of various samples. Because of the pitting potential [30], a static attuide was sought to investigate the effect of grain size on pitting potential of AA6061 Al.

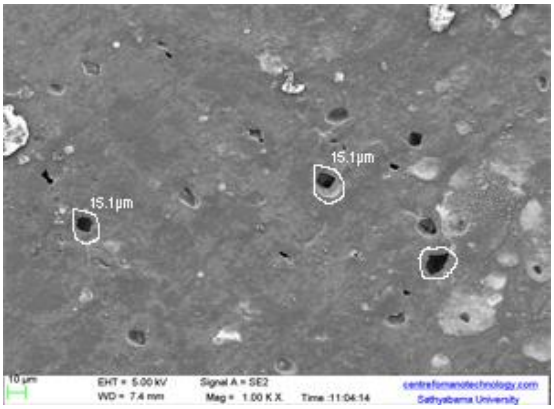

Fig.3. Morphology and location generated metastable pits on an alloy with average grain size of 15.1µm after the low scan ratepotentiodynamic polarisation test

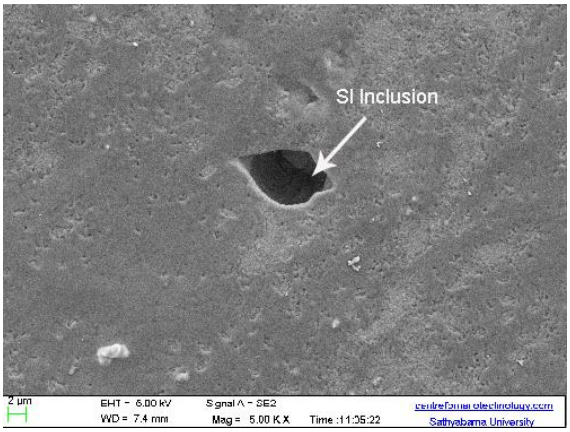

Fig. 4. Scanning Electron microscope (SEM) of a silicon inclusion as a pit initiation site

3. METASTABLE PITTING

The early development of stable pit is identical to that of metastable pit [16], and the probability of stable pitting is directly related to the metastable pitting characteristics [17]. From metastable pitting studies, many aspects of stable pitting can be understood. In an effort of providing fundamental information about the influence of grain size on the metastable pitting initiation and on the transition from metastability and stability, potentiostatic tests were conducted at three constant potentials.

Metastable pit initiation.Metastable pit frequencies, i.e the number of metastable pit events per surface area divided by time Period which they are counted (100s) obtained from the potentiostatic polarisation of 6061 Al and sample with different grain size are plotted versus time at various potentials. Generally, an increase in the grain size causes a decrease in the frequency of metastable pit events in each given potential. The major parts of metastable pitting activities are observed in the initial time of the test, which is mostly decreased expeditiously with time which believed to be associated with a decrease of the total number of surface sites available for metastable pitting.[19]

Metastable pit Initiation. It is clear that grain refinement decreases the number of metastable pits that can be generated. An improved passive film with grain refinement has been reported in the large range of metals [21-24]. Passive film in Fe alloys is

termed as being more electrochemically stable with a higher diffusion rate than coarser grained microstructures [21-23].The enhanced diffusion of Cr into the passive film causes a chromium-rich protective film to build up. Finer grain 6061Al has a high density of grain boundaries for forming a passive layer having more chromium. In other words, since the fine-grained structure has higher grain boundaries density, they have more fraction of surface area which the passive film formed over is more stable. Besides the distribution of SI sulphide inclusion as susceptible sites of pit nucleation [25] does not change with grain refinement, thus it is probable that finer grained structured alloy, more nucleation sites would be located at grain boundaries which are capable to form a more stable passive film. Hence the frequency of metastable pit initiation is reduced by grain refinement. The upward trend of metastable initiation frequency with potentials has been reported by other researchers [26-28]. Increasing the pit initiation frequency with an increase in potential could be explained based on some major influences of potential. The current densities in pre-existence flaws increase with applied potentials and consequently, active corrosion is initiated at the bottom of the flaws . Pistorius and Burstein [29] have suggested that more open sites, which allowed faster diffusion rate, are only susceptible to initiation at higher potentials because the dilution of pit electrolyte could be prevented by higher active solution rate. Furthermore, by increasing the potentials, the surface is becoming more positive and attraction of negative ions to the surface would be facilitated.

Table-1-Chemical Composition of ALUMINIUMAA6061-T6

ELEMENTS	SI	FE	CU	Mn	Cr	AL
WT %	0.708	0.212	0.184	0.127	0.098	Remainder.

Table-2-Chemical Composition Pure Copper

ELEMENTS	CU	Pb	Sn	Fe	Ni	Te
WT %	99.73	0.003	0.184	0.080	0.068	0.018

Table-3-Chemical Composition of Nickel

ELEMENTS	Al	Mn	Si	Mo	Cr	Ni
WT %	0.033	0.003	0.002	0.004	0.002	99.5

Table 4

Sl. No.	**Upset Pressure (in tons)**	**Friction Pressure (in tons)**	**Burn off length (in mm)**	**Speed of Spindle (in rpm)**	**Remarks**
1	2.5	1.3	1	2000	Cu doesn't weld
2	2.6	1.5	2	1000	Cu doesn't weld
3	2.7	1.7	3	1500	Cu came out on machining
4	**2.8**	**1.8**	**2**	**1500**	
5	**2.9**	**1.9**	**3**	**2000**	
6	**3.0**	**1.9**	**1**	**1000**	
7	**2.0**	**2.0**	**3**	**1000**	
8	3.1	2.1	2	1500	Cu came out on machining
9	3.2	2.2	2	2000	Cu doesn't weld

Out of these parameters, a few parameters did not give satisfactory results as given in the remarks column of Table 4 and have been omitted from the remaining part of the experimental work. Only the parameters which gave satisfactory results have been chosen for corrosion testing. These parameters are shown in Table 5

Table 5

The friction welding parameters used for this work are as shown below in Table 4.

S No	**Sample no**	**Friction pressure (MPa)**	**Upset pressure (MPa)**	**Burn-off length (mm)**	**Speed (RPM)**
1	4	2.8	1.8	2	1500
2	5	2.9	1.9	3	2000
3	6	3.0	1.9	1	1000
4	7	2.0	2.0	3	1000

.Hence, these parameters were used to prepare specimens for corrosion testing.

4. RESULTS AND DISCUSSION

Table-5

Sample No	I corr mA/Sq cm	Rest potential	Reverse potential	Corrosion rate	Remarks
4	37.408	-722.46	250 mV	870.12(mm/year 34256(mil/year	Cu-Ni-Al
5	36.69	-721.96	250 mV	412.03(mm/year 16221(mil/year	Cu-Ni-Al
6	356.64	-728.03	250mV	8295.5(mm/year 326590(mil/year	Cu-Ni-Al
7	**0.4659457**	**-733.97**	**250mV**	**5.2325(mm/year 206.0(mil/year**	**Cu-Ni-Al**
Cu Base metal	209..37	-291.99	250mV	4870.1(mm/year) 191730 (mil/year)	Cu
Al Base metal	558.82	-734.65	250mV	6275.5(mm/year) 247070(mil/year	Al
Nickel Interface metal	0.00285	-335.37	250mV	0.030664(mm/year) 1.2072(mil/year)	Ni

The parameters used in the friction welding of sample No: 7 Cu-Ni-Al showed lowest corrosion rate and the corresponding Corrosion current (ICorr) is also lower. The corrosion current is as low as 0.466 mA/Square centimeter.

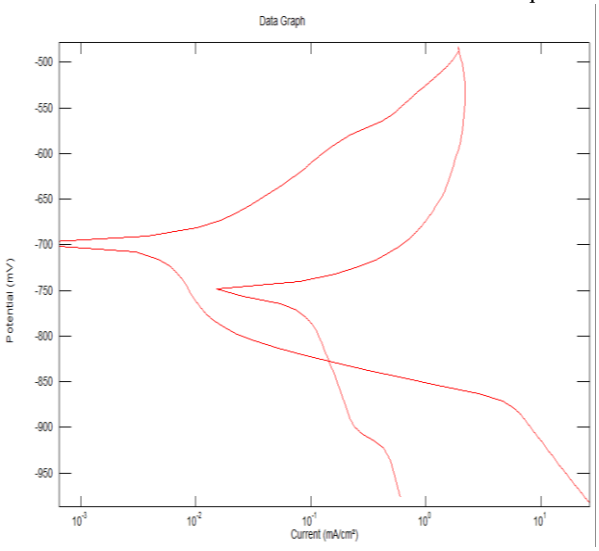

Fig.5.Polorization Curve Al –Ni-Cu (Sample. No-7)

The highest corrosion rate is shown by sample No: 6 at the interface. The corrosion current Namely ICorr is as high as 356.64 mA/ Square centimeter. Sample 6 has a friction welding parameter combination of high friction pressure, low burn off a length and lower speed of rotation.It is possible that higher friction pressure led to greater sites of corrosion initiation. Lower burn off length also leads to lesser bonding at the interface. Generally, lower speed of rotation leads to better welds. Hence, the loss of bond strength due to using lower burn off could have been compensated by the use of the low speed of rotation

On the other hand the sample No: 4 & 5 showed corrosion in the inter-mediate range. The corrosion current is 37.408 & 36.69 m A/ Square centimeter. The corresponding corrosion rate is 870.12 mm & 412.03 mm per year respectively.

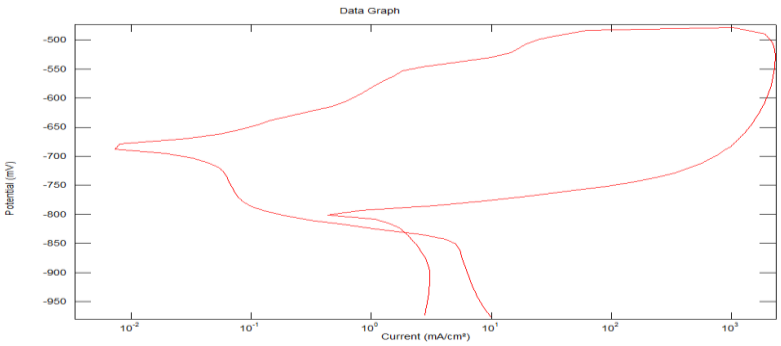

Fig.6. Polarization curve Al-Ni- Cu (SAMPLE No.6)

The surface of the potentiodynamic polarization subjected shows deep corrosion pits for sample No:6. Compared to sample No:6 the sample No: 7 friction welded surface interface showed lowest pits and corrosion affected areas. On the other hand the sample NO: 4 & 5 showed severe oxidized surface by the corrosion tests. The black surface appearing in the image is the deep oxidized zones and the depth of the pits is higher. The parameters used for the sample No; 7 seemed to be effective as it has produced the lowest corrosion current and corrosion rate. Hence the parameters of 2 bar upset pressure followed by friction pressure of 2 bar with the burn of the length of 3 mm at 1000 RPM is ideal among the various parameters of friction welding used in this study.

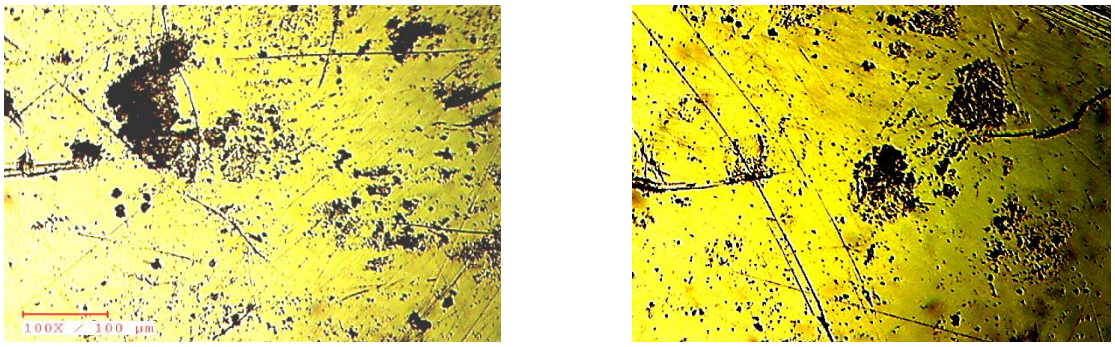

Fig. 7. Microstructure Al-Ni-Cu (sample No7) (after corrosion)

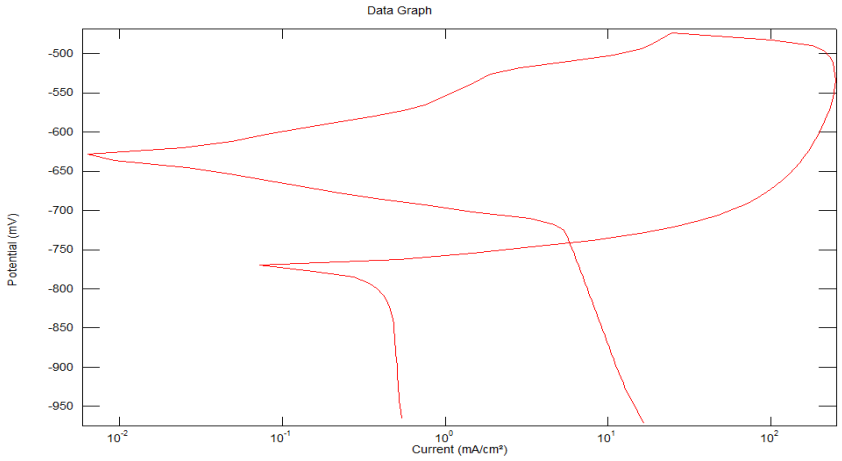

Fig. 8. Polarization curve Al-Ni-Cu

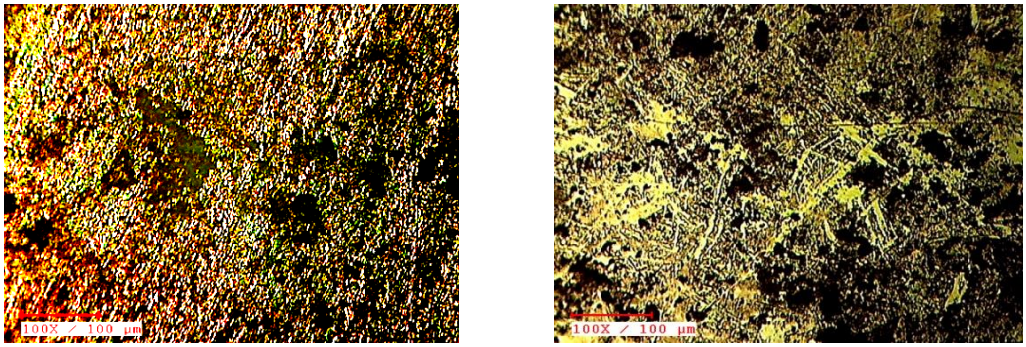

Fig.9. Microstructure Al-Ni-Cu (sample- 4) (after corrosion)

Comparison of the potentio dynamic polarization values shows that Nickel base metal is least affected and values are very low. The corrosion current value is least as the metal show high resistant to the polarization and show high resistant. It is seen from the above corrosion tests the corrosion parameters obtained for all the interface in which Nickel is interfaced the corrosion at the nickel interface would be lowest. Sample No-7 where the nickel as the interface showed lowest corrosion rate as nickel resisted the corrosion by polarization. Hence the parameter used in the above friction welding studies show that the sample No-7 with the upset pressure of 2, friction pressure of 2Mpa and burn of the length of 3mm seemed to be optimum parameters to be used for lower corrosion and welding.Comparison of the microstructure of the corrosion tested specimen shows that the pure nickel showed very low corrosion products and corrosion boundaries and pits. Similarly sample No; 7showed considerable less corrosion affected surface compared to other parameters of sample No: 4, 5, and 6.

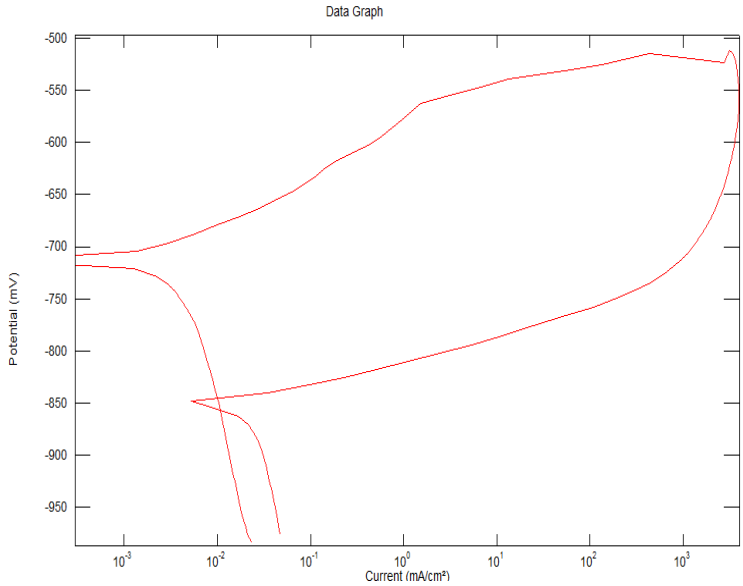

Fig. 10. Base metal Aluminum alloy Analysis of the curve

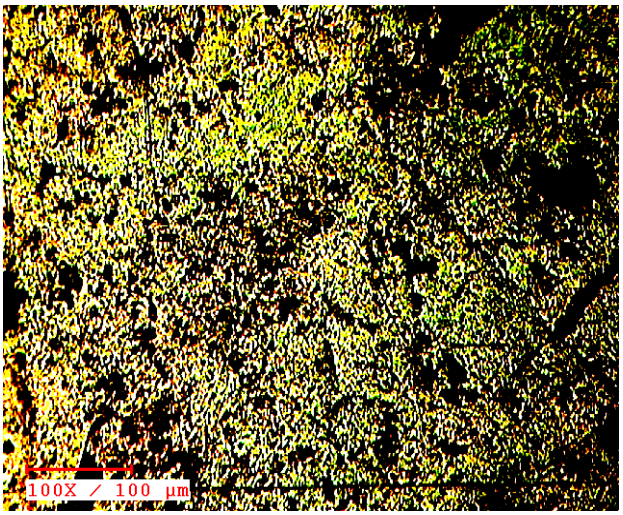

Fig. 11. Microstructure Al (After corrosion)

David Talbot and jamesTabolt [9] studied the passive oxide film that is easily formed on the surface of Aluminum alloy when it is exposed to air or water due to the presence of chloride ions. Kenneth R et al also revealed that in the presence of chloride ions the corrosion rate is very high. Another factor which affects corrosion rate ishetrogenety of their microstructure [10] Polarization resistance can be related to the rate general corrosion of metals at or near their corrosion potential, Ecorr. Polarization resistance measurements are an accurate and rapid way to measure the general corrosion rate. Electro chemical polarization methods are extremely pertinent for understanding and evaluating the corrosion resistance of materials and the effect of changes in the corrosive environment. They can establish criteria for anodic or catholic protection and susceptibility to several forms of corrosion. Venugopal et al[11] studied microstructural and pitting corrosion properties of friction stir weld 0f AA7075 AL alloy in3.5% NaCl solution. Corrosion resistance of weld metal is better than that of TMAZ and base metals. Srinivasarao and Prasad rao[12] studied the mechanism of pitting corrosion test by Tafel curve extrapolation method was carried out for samples 6 and 7. Samples of base alloy AA6061 and Ni and friction welded area in solution chloride of 3.5 % to determine corrosion parameter such as corrosion potential (Ecorr) and corrosion current (Icorr) as shown in Table 5.

SEM ANALYSIS

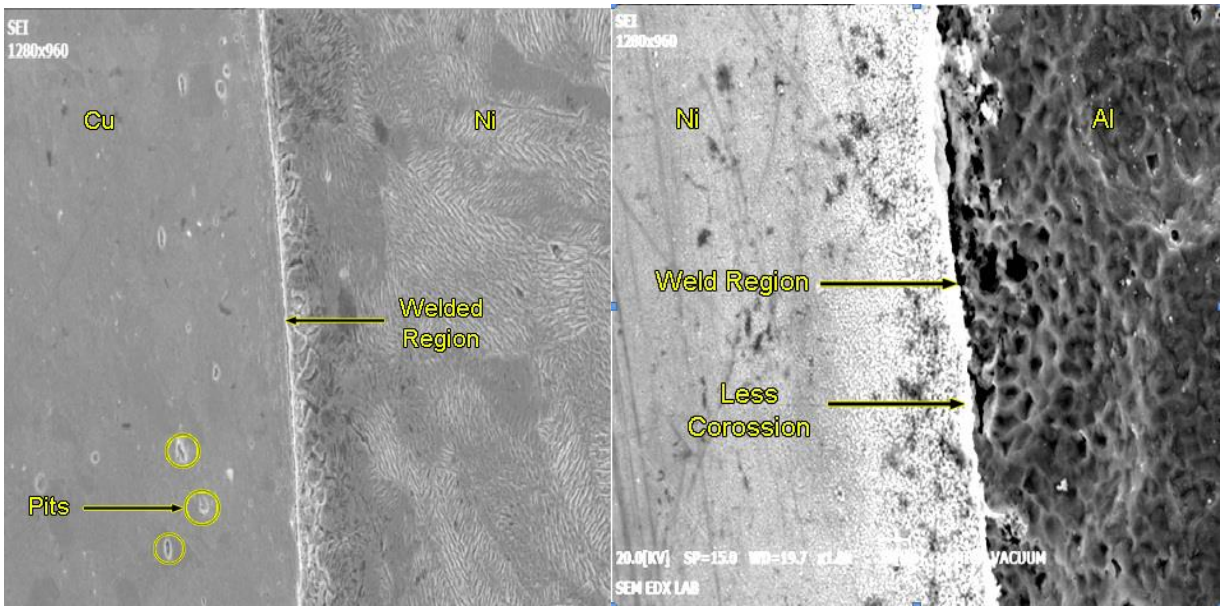

(a)-Cu-Ni (b)-Ni-Al

Fig.12: (a) & (b) SEM Images for Sample 7

The interface zone of the process after the corrosion test. Corrosion products formed along the copper boundary side of the Aluminium-Nickel-Copper friction weld at the interface and small pits distributed near the interface (shown in fig 7 a) is a remnant of the passive film[13].Stewart and Williams [14] also showed that inclusions dominate as pit nucleation sites, and the lifetime of a metastable pit is directly related to the size of the inclusion particle.Osozawa and Okato[15] found that pitting potential depend on the size of the largest inclusion present in the stainless steel.

Fig 7(b) interface zone of the nickel and AA 6061 Aluminium alloy. The corrosion attack is least at the fusion & interface zone. The corrosion pits are finer and not deep compared to the other samples at the same location. At the same time nickel is not affected as compared to Aluminium alloy.

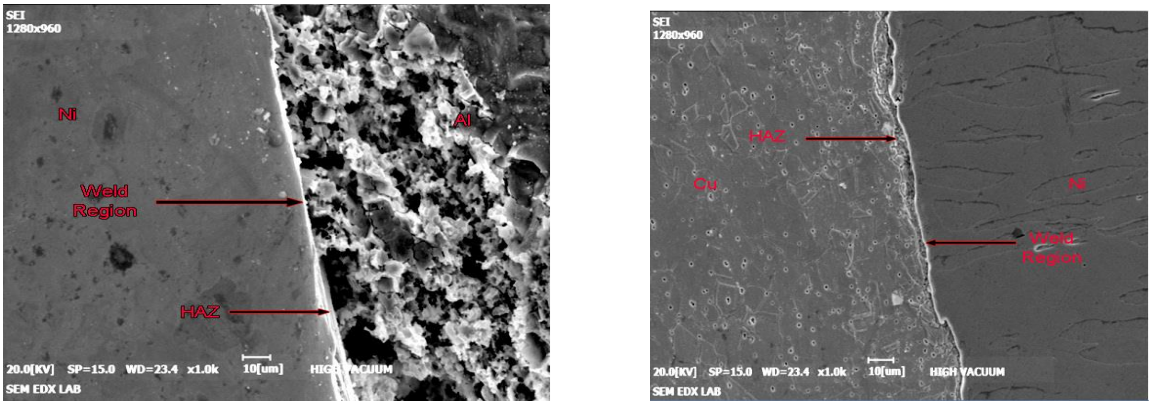

(a) (b)

Fig.13.SEM images for sample 6

SEM photographs show the interface zone of the process after the corrosion test. Corrosion products formed along the copper boundary side at the interface. (a) The interface zone of the nickel and AA 6061 Aluminum alloy. The corrosion attack is more in the fusion zone leading to the formation of deep pits along the interface. This is because welding is not complete.

Macro analysis

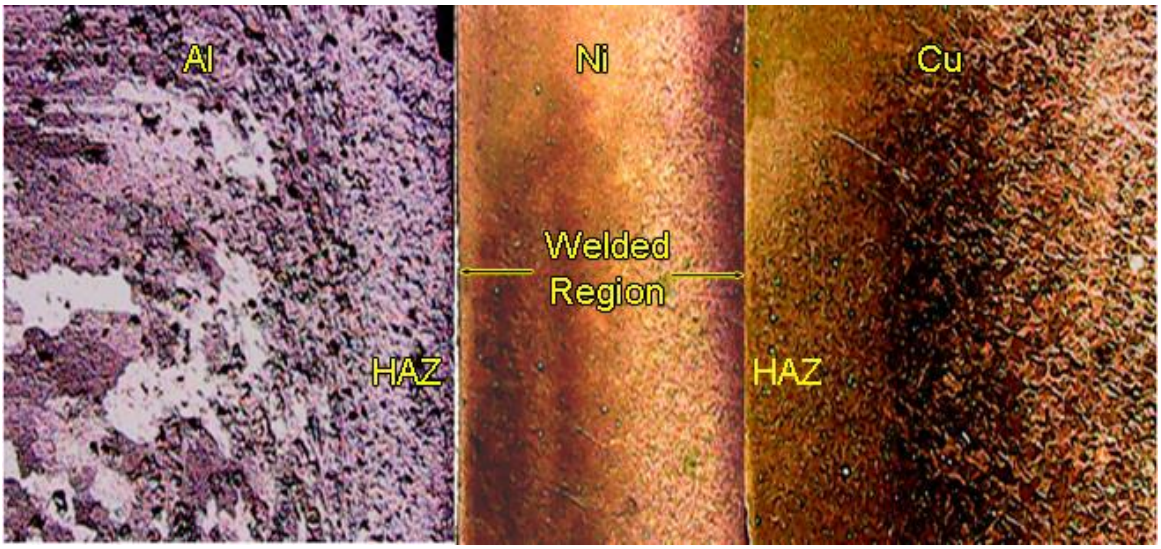

Fig.14. friction welded Al-Ni-Cu (Sample 7)

The copper shows more heat affected zone compared to the other two metals. The Aluminium alloy shows the good flow of grains under pressure and heat of the process. Re-crystallization is effected as the grains are clearly resolved. At the heat affected zone, the dissolution of the eutectic particles has taken place as no grains of eutectics observed. The heat of the process affected some re-crystallization near the heat affected zone. The nickel shows fine pitting marks probably due to excessive heat input. The heat affected zone of the copper shows fine grains on macro etching. A layer of copper has plastically deformed found between the nickel and aluminum alloy interface.

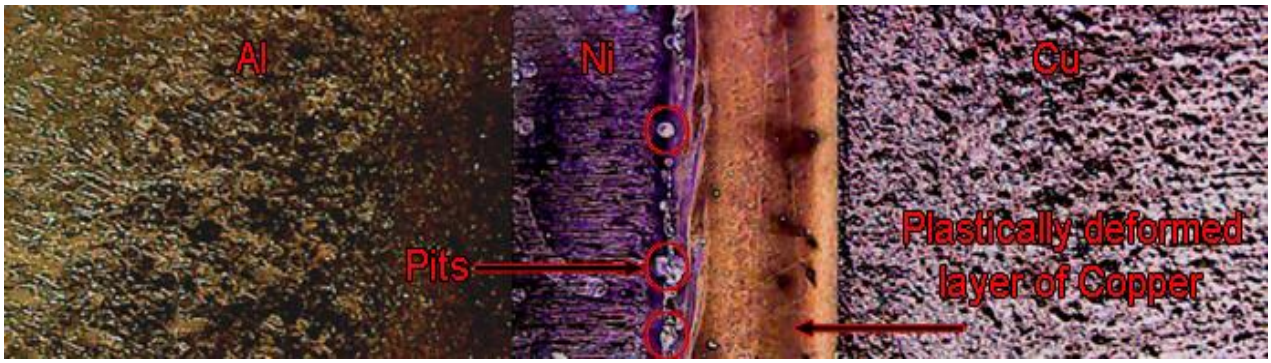

Fig. 15. Friction welded Al-Ni-Cu (Sample 6)

The copper shows a higher thickness of heat affected zone compared to the other two metals. The Aluminum alloy shows the good flow of grains under pressure and heat of the process. The heat of the process affected some re-crystallization near the heat affected zone. The nickel shows fine pitting marks probably due to high heat input. The heat affected zone of the copper shows fine grains on macro etching. A layer of copper which is plastically deformed found between the nickel and aluminum alloy interface.

5. CONCLUSIONS

The work investigated corrosion behavior of Ni interlayer on Aluminium -Copper. The findings made by the experimental work are given below.

- Potentio dynamic polarization test it reveals that sample 7 shows low corrosion rate of5.2325(mm/year) and sample 6 shows high corrosion rate.(8295.5(mm/year).
- The resting potential is high at the weld, thermo mechanically affected zone and heat affected zone which has the high resistance to corrosion compared to the parent metal.
- Potentiodynamic measurements conducted in 3.5 wt% sodium chloride solution revealed that grain size variation has no considerable effect on pitting potential of AA6061 Aluminium.
- The corrosion attack is severe in the fusion zone leading to the formation of deep pits along the interface as seen in SEM analysis of sample 6 compared to sample 7.
- The Aluminium matrix with fine pits is uniformly spread due to the corrosion process by the electrolyte. More pits could be seen in the matrix compared to the samples with Nickel interlayer.

6. ACKNOWLEDGE MENT

The authors thank Dr.Sathikh, former vice-chancellor Madras University, Met Mechlab Chennai for the experimental work and I.I.T Chennai for friction welding. They also thank the Management, Sathyabama University, St. Joseph's College of Engineering, Chennai and SSN College of Engineering.

7. REFERENCES

[1] B. S Yilbas, A. ZSahin , N. Kahraman, and A.Z.Al- Gami: J. Mater. Process. Technol, 49 (1995)
[2] G.Mahendran, V.Balasubramanian,T.Senthilvelan, Influences of diffusion bonding process parameters on bond characteristics of Mg-Cu dissimilar joints, Trans.Nonferrous Met.Soc.China,2010,20,p997-1005
[3] Won-B. Lee, Kuck- saeng Bang,Seung- Boo Jung Journal of Alloys of compounds, 390 (2005)
[4] Garcia C, Martise F, De Tiedra P, Blanco Y, Lopez M, Corros sci2008:50:1184-94
[5] BilmesPD,Llorente CL, Mendez CM, Garvasi CA CorrosSci 2009;51:876-81
[6] J G Kaufman and E.L Rooy, corrosion test and standards, Applications and Interpretation,2nd edition, edited by R. Baboian, ASM International, Material park, OH, (2005) 1-8.
[7] J. G. Kufman, in ASM Hand book, Volume 13 B, Corrosion: Materials,edited by S.D. Cramer and B.S. Covino Jr. ASM International, Material park,OH (2005) 95 -124.
[8] I.J Park,S.T Kims, I.S. Lee, Y.S. Park, M.B.Moon,Mater. Trans. (JIM) 50 (2009)
[9] David Talbot and james Talbot, Corrosion Science and Technology,CRC Press LIC,1998
[10] R Kenneth, Trethwey and J.Chamberlain,Corrosion for Science and Engineering, Long man Group limited,2nd Edition,1996.
[11] T.Venugopal,K. Srinivasarao,andK.Prasadrao, Trans Inst. Metals, 57(2004) 659-663.
[12] K.Srinivasa Rao and K.Prasad Rao, Transaction of Indian Institute of metals, 57(2004) 503-610.
[13] G.S Frankel, L. Stockert, F,Hunkeler, H.Boehni,Metastable Pitting of Stainless Steel, Corrosion43 (1987) 429-436.
[14] P.C .Pistorius, G.T Burstein,Corros.Sci. 33 (1992) 1885-1897.
[15] J Stewart, D.E .Williams, Coros. Sci 33(1992) 457-463.
[16] G. Daufin. J. pagetti,J.P.Labble,F Michel, Pitting Initiation on stainless steel: electrochemical and micrographic aspects, corrosion 41 (1985) 533-539.
[17] J.Liu, T. Zhang, G. Meng, Y. Shao, F. Wang, Effect of pitting nucleation on critical pitting temperature of 316L Stainless steel by nitric acid passivation, Corros. Sci, 91 (2015) 232-244.
[18] P.C Pistorius, G.T. Burstein, Growth of Corrosion pits on stainless steel in choloride solution containing dilute sulphate, Corros. Sci 33 (1992) 1885-1897.
[19] G.O IIevbare, G.T. Burstein, The inhibition of pitting corrosion of stainless steel by chromate and moiybdate ions, corros. Sci.45 (2003) 1545-1569.
[20] A . Di Schino, J. M. Kenny, Effect of the grain size on the corrosion beheaviour of refined AISI 304 austentic Stainless Steel, J. Matter . Sci. Lett.21 (2002) 1631- 1634).
[21] B. Hadzima, M. Janecek, Y. Estrin, H.S Kim, Microstructure and corrosion properties of ultrafined – grained interstitial free steel. Master Sci.Eng. A 462 (2007) 243-247.
[22] X.Y. Wang, D.Y.Li Mechanical and electrochemical beheaviour of nanocrystalline surface of 304 Stainless steel, Electrochem. Acta 47 (2002) 3939- 3947.
[23] W. Zeiger, M. Schneider, D. Scharnweber, H. Worch , Corrosion beheaviour of a Nanocrystalline FeA18 alloy. Nanostruct. Mater. 6 (1995) 1013-1016.
[24] K.M.S. Youssef, C.C Koch, P.S. Fedkiw, Improved corrosion beheaviour of nano crystalline zinc produced by pulse- current electodeposition, corros. Sci, 46 (2004) 51-64.
[25] G. Wranglen, pitting and sulphide inclusion in steel, Corros. Sci 14 (1974) 331-349.
[26] D.E Willaims, J. Stewart, P.H. Balkwill, The nucleation, growth and stability of microptic in stainless steel, Corros. Sci 36 (1994) 1213 -1235.
[27] M.H Ras , P.C. Pistorius, possible mechanism for the improvement by vanadium of the pitting corrosion resistance of 18% choromium feritic Stainless steel, Corros.Sci.44 (2002) 2479 -2490.
[28] W Tain, N. Du, S. Li, S. Chen, Q wu, Metastable pitting corrosion of 304 Stainless steel in 3.5% NaCl solution. Corros. Sci 85 (2014) 372-379.
[29] P.C. Pistorius, G.T. Bustein, Aspect of the Effect of electrolyte composition on the occurrence of metastable pitting on stainless steel, Corros. Sci 36 (1994) 525-538.
[30] B. YU, P. Woo, U. Erb, Corrosion behavior of nanocrystalline copper foil in sodium hydroxide solution, Scr. Mater. 56 (2007) 353-356.

